





## Electrocatalytic detection of L-cysteine using molybdenum POM doped-HKUST-1 metal organic frameworks

Tafadzwa W. Murinzi<sup>a,b</sup>, Gareth M. Watkins<sup>a</sup>, Munyaradzi Shumba<sup>b,c</sup>  and  
Tebello Nyokong<sup>c</sup> 

<sup>a</sup>Chemistry Department, Rhodes University, Grahamstown, South Africa; <sup>b</sup>Chemical Technology Department, Midlands State University, Gweru, Zimbabwe; <sup>c</sup>Nanotechnology Innovation Centre, Rhodes University, Grahamstown, South Africa

### ABSTRACT

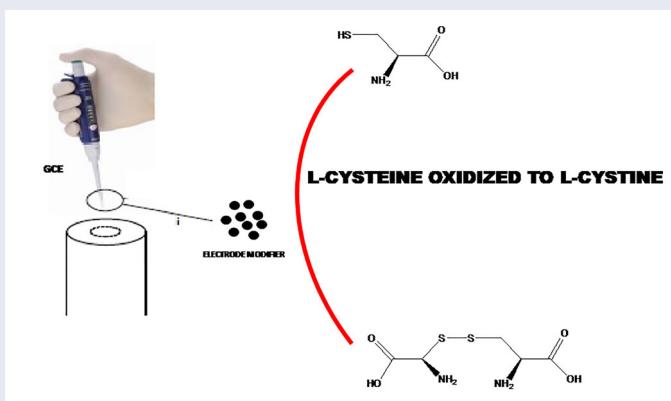
Glass carbon electrodes (GCE) were modified with metal organic frameworks (MOFs) containing molybdenum polyoxometallates (Mo POMs) in a copper benzene tricarboxylate framework (HKUST-1). The Mo POMs were introduced via one-pot synthesis (Mo2) and post-synthetic modification (Mo1) techniques. The electrode modifiers were characterized by powder X-ray diffraction (PXRD), Fourier transform infrared spectroscopy (FTIR), scanning electron microscopy (SEM), and thermal analysis. The modified electrodes' oxidation capacity toward L-cysteine was studied. Mo POMs significantly improved electron transfer kinetics compared to the bare GCE. The best Mo POM doped electrode (Mo1-GCE) had a catalytic rate constant of  $2.2 \times 10^4 \text{ M}^{-1} \text{ s}^{-1}$  and a limit of detection of  $3.07 \times 10^{-7} \text{ M}$ . Under the employed experimental conditions, the detection response for L-cysteine was very fast (within 0.1 s) for all the modified electrodes and selective toward L-cysteine in the presence of other amino acids.

### ARTICLE HISTORY


Received 30 November 2020  
Accepted 18 February 2021

### KEYWORDS

Molybdenum polyoxometal-  
lates; metal organic  
frameworks; electrocatalysis;  
host-guest electrochemistry



CONTACT Munyaradzi Shumba  [shumbamunya@staff.msu.ac.zw](mailto:shumbamunya@staff.msu.ac.zw),  [mmubaiwash@yahoo.com](mailto:mmubaiwash@yahoo.com)

 Supplemental data for this article can be accessed online at <https://doi.org/10.1080/00958972.2021.1907573>.

© 2021 Informa UK Limited, trading as Taylor & Francis Group

## 1. Introduction

Molybdenum polyoxometallates (Mo POMs) are well known for their redox properties and are often chosen as candidates for heterogeneous catalysts [1, 2]. Due to their high catalytic activity, Mo POMs have been employed as catalysts in the oxidative desulphurization of fuels [3, 4], in the synthesis of oxazolines and thiazolines [5], and as electrocatalysts for various chemical species such as nitrates and hydrogen gas [6–8]. In most of these applications, POMs are loaded onto porous materials such as zeolites since on their own, they are prone to aggregation which reduces the accessible surface area [9]. There is therefore need to immobilize Mo POMs on a porous matrix in order to fully exploit their catalytic properties. Metal organic frameworks (MOFs) are attractive candidates for Mo POM immobilization due to their larger surface areas, tunable properties and higher stabilities [10–12].

HKUST-1 ( $\text{Cu}_3(\text{BTC})_2(\text{H}_2\text{O})_n$ ) is an example of a MOF with most of these desirable properties. It has a Brunauer-Emmett Teller (BET) specific surface area of  $1055 \text{ m}^2/\text{g}$  and a pore size of  $9 \text{ \AA} \times 9 \text{ \AA}$  [13–15]; because of the latter, it has been employed as a matrix for other materials. For example, HKUST-1 has been used as a matrix to synthesize CuO and CuO-CeO<sub>2</sub> nanoparticle catalysts for CO oxidation [16]. It has also been used for encapsulation of Fe<sub>3</sub>O<sub>4</sub> nanocomposites for oxidation of benzylic C–H bonds [17] and for storage of gases (H<sub>2</sub>, N<sub>2</sub>) [18]. In addition to their matrix applications, when combined with other metals MOFs create synergistic effects on the properties of the resulting product, making them highly sought after candidates especially as catalysts [7]. Carbon functionalized MOF Nafion composites have been used for dopamine sensing [19]. Polyoxometallates (POMs) have been used as electrocatalysts due to the high oxidation states of the metals [20]. The combination of Cu and Mo centers in an electrocatalyst for reduction of nitrate has been successful for a small polyoxomolybdate (Mo<sub>2</sub>) [7]. Based on their previous successes, HKUST-1 was selected for this work to exploit its stability as a matrix and Mo POMs were selected for their catalytic potential creating Mo POM-HKUST-1 hybrid materials.

L-cysteine is an amino acid that is important for various metabolic processes such as protein synthesis [21], detoxification, and antioxidant activity [22]. The sulfhydryl group in L-cysteine also plays a vital role in enzyme catalytic activity [23]. In tissue proteins and blood, L-cysteine mainly exists as the oxidized form, L-cystine. Inside cells, however, L-cystine is the prevalent form due to the reducing environment [24]. A balance has to be maintained between the intracellular and extracellular environment. Imbalance of extracellular L-cysteine/L-cystine is associated with oxidative stress and other pathological disorders. These can be avoided by monitoring L-cysteine levels resulting in improvement in human health. Monitoring can be achieved via biological sensors [25]. Numerous attempts have been made to detect L-cysteine using various techniques; very few, however, use MOFs in electrochemistry [26–28]. This work was an attempt at using the larger polyoxomolybdates (Mo<sub>6</sub>) incorporated into HKUST-1 MOF to give Mo<sub>6</sub>-CuBTC POM-MOF hybrids to be employed as biosensors for L-cysteine.

## 2. Experimental

### 2.1. Materials

Buffer tablets of pH 4 were purchased from Saarchem.  $\text{Cu}(\text{NO}_3)_2 \cdot 3\text{H}_2\text{O}$ , benzene tricarboxylic acid ( $\text{H}_3\text{BTC}$ ), ammonium heptamolybdate tetrahydrate (AHM), L-cysteine, glutamic acid, glutamine, lysine, tyrosine, phenylalanine, leucine, alanine, glycine, alumina ( $10\ \mu\text{m}$ ), ethanol, and dimethylformamide (DMF) were purchased from Sigma Aldrich. Millipore water dispensed from Milli-Q Water Systems (Millipore Corp. Bedford, MA, USA) was used for all aqueous preparations. All chemicals were used as supplied.

### 2.2. Equipment

IR spectra were recorded from  $4000$  to  $400\ \text{cm}^{-1}$  on a Perkin-Elmer Spectrum 400 FTIR/FT-FIR Spectrometer. Elemental analysis was carried out using an Elementar Vario Micro cube with a thermal conductivity detector (TCD), employing temperatures of  $1150^\circ\text{C}$  in the combustion tube and  $850^\circ\text{C}$  in the reduction tube. Helium ( $1200$ – $1350$  mbar) and oxygen ( $17$  mbar) were used as the gases. SEM images were collected using a TESCAN Vega TS 5136 electron microscope. X-ray powder diffraction (PXRD) spectrum was performed on a Bruker D8 Discover diffractometer, equipped with a LynxEye detector, under Cu-K $\alpha$  radiation ( $\lambda = 1.5405\ \text{\AA}$ ). Data were collected from  $2\theta = 10^\circ$  to  $60^\circ$ , scanning at  $0.010^\circ\ \text{min}^{-1}$  and  $192\ \text{s}$  per step. All TGA studies were conducted using a Perkin-Elmer TGA 4000. Between  $2.5$  and  $5.0\ \text{mg}$  of sample was placed in a ceramic crucible and loaded in the TGA furnace. The sample was heated under nitrogen to  $30^\circ\text{C}$ , held for  $1$  minute and then heated from  $30$  to  $800^\circ\text{C}$  at a rate of  $10^\circ\text{C}/\text{min}$ . DSC was performed on a Perkin-Elmer DSC 6000. Between  $2.5$  and  $5\ \text{mg}$  of sample was loaded into alumina pans and heated with a ramp rate of  $10^\circ\text{C}/\text{min}$  from  $30$  to  $445^\circ\text{C}$  under nitrogen. All electrochemical experiments (cyclic voltammetry and chronoamperometry) were performed using CV BAS 50.

### 2.3. Synthesis

#### 2.3.1. Synthesis of HKUST-1

HKUST-1 was synthesized under solvothermal conditions, as detailed below by the literature procedure [18]. Copper nitrate trihydrate ( $0.6\ \text{g}$ ,  $2.48\ \text{mmols}$ ) was dissolved in  $10\ \text{mL}$  of distilled water. Benzene tricarboxylic acid ( $\text{H}_3\text{BTC}$ ) ( $0.4\ \text{g}$ ,  $1.9\ \text{mmols}$ ) was dissolved in  $10\ \text{mL}$  of a 1:1 mixture of ethanol and distilled water in a separate beaker. The two solutions were combined and placed in an ultrasonicator until a gelatinous blue substance was formed. The gel was placed in a glass vial, sealed and placed in an autoclave. The autoclave was heated to  $120^\circ\text{C}$ , maintained at this temperature for  $24\ \text{h}$ , and then cooled to room temperature, at which point turquoise blue HKUST-1 crystals had formed. The crystals were filtered off, washed with  $20\ \text{mL}$  of a 1:1 ethanol:water solution and dried in an oven for  $12\ \text{h}$  at  $60^\circ\text{C}$ .  $\text{Cu}_3(\text{BTC}) \cdot 3\text{H}_2\text{O}$  ( $451.64\ \text{g}$ ): calculated C  $33.745$ , H  $0.021$ , Cu  $29.758$ ; found C  $33.250$ , H  $0.018$ , Cu  $30.080$ .

**2.3.1.1. Post-synthetic modification (PSM) of HKUST-1 to form Mo1.** The HKUST-1 samples were then modified via impregnation. Impregnation was achieved by sonicating

**Table 1.** Electrochemical parameters for the bare and modified electrodes.

GCE modifier	$\Delta E_p$ for $\text{Fe}(\text{CN})_6^{3-/4-}$ in 0.1 M KCl	E/V (L-cysteine) oxidation pH 4 buffer	Surface roughness	Eff. Area	$\Gamma$ (mol $\text{cm}^{-2}$ )	Background corrected oxidation currents/ $\mu\text{A}$ in pH 4 buffer	Current density/ $\mu\text{A cm}^{-2}/V$
Bare GCE	0.078	–	–	–	–	–	–
HK-GCE	0.226	0.283	7.5075	0.533	$5.51\text{E} - 11$	39.75	74.58
Mo1-GCE	0.110	0.205	16.8168	1.194	$1.40\text{E} - 11$	31.40	26.30
Mo2-GCE	0.132	0.328	8.5886	0.609	$2.45\text{E} - 11$	58.60	96.20

HKUST-1 (0.2 g) with ammonium heptamolybdate (0.6 g, 0.485 mmols) in 20 mL ethanol for 2 h, followed by filtering and drying of the precipitate in an oven at 60 °C for 12 h. The resulting blue-green crystals are referred to as Mo1.  $\{\text{Cu}_3(\text{BTC})_2(\text{H}_2\text{O})_3\} \cdot 3\frac{1}{2}[(\text{NH}_4)_6\text{Mo}_7\text{O}_{24} \cdot \frac{1}{2}\text{H}_2\text{O}]$  (4762.93 g): calculated C 4.535, H 2.090, N 6.172, Cu 4.00, Mo 49.356; found C 4.250, H 1.891, N 5.920, Cu 3.875, Mo 49.720.

### 2.3.2. One-step solvothermal synthesis of Mo2

Copper nitrate trihydrate (0.6 g, 2.48 mmols) and  $\text{H}_3\text{BTC}$  (0.4 g, 1.9 mmols) were dissolved in 10 mL of a 1:1 mixture of ethanol and millipore water. Ammonium heptamolybdate tetrahydrate (0.6 g, 0.485 mmols) was placed in 10 mL millipore water and heated with stirring until it dissolved. The two solutions were combined and sonicated until a gelatinous blue substance was formed. The gel was placed in glass vial, sealed and placed in an autoclave at 180 °C for 24 h. The resulting gray crystals were slowly cooled to room temperature, filtered off, and washed with 20 mL of a 1:1 mixture of ethanol and water. The product, referred to as Mo2, was dried overnight in an oven at 60 °C.  $\text{Cu}_{5\frac{1}{2}}(\text{BTC}) \cdot (\text{NH}_4)_6\text{Mo}_7\text{O}_{28} \cdot 5\text{H}_2\text{O}$  (1874.15 g): calculated C 5.763, H 1.974, N 4.482, Cu 18.650, Mo 35.837; found C 5.550, H 1.801, N 4.299, Cu 18.880, Mo 36.001.

## 2.4. Electrode modifications

A glassy carbon electrode (GCE) was used as the working electrode, a silver/silver chloride wire was used as a pseudo-reference electrode and a platinum wire was used as the counter electrode. The GCE was polished on a Buehler-felt pad using alumina (<10  $\mu\text{m}$ ). Between each polishing step, impurities were removed by sonicating for 5 min in millipore water. The electrode was rinsed in millipore water, dried and modified using the dip dry method. For each of the modifiers, an optimum concentration of 2 mg/mL modifier in DMF was sonicated for 30 min. The electrode was then dipped in the suspension and dried in an oven at 70 °C. The electrodes are designated as HK-GCE, Mo1-GCE, and Mo2-GCE after modification with HKUST-1, Mo1, and Mo2 suspensions, respectively. A complete list of the electrodes is shown in Table 1.

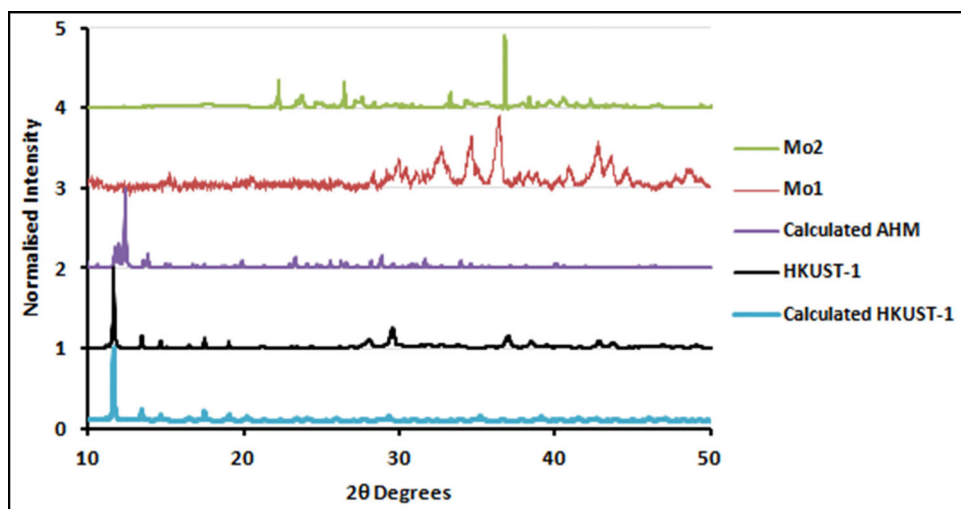


Figure 1. PXRD spectra of HKUST-1, Mo1, Mo2, and AHM.

### 3. Results and discussion

#### 3.1. Characterization by PXRD

The MOF HKUST-1 has been synthesized before and characterization was performed to confirm that synthesis was successful [13–15]. A lower temperature of 120 °C (versus 180 °C [29]) was used to avoid the formation of cuprous oxides in the potential voids [13, 14, 30]. The crystals had the characteristic turquoise blue color and the HKUST-1 PXRD pattern (Figure 1) matches those reported (Figure 1 – calculated HKUST-1 by Chui [29]) with peaks at  $2\theta = 11^\circ$ ,  $13^\circ$ ,  $17^\circ$ , and  $29^\circ$  [13, 31, 32]. A more concise comparison between the as-synthesized and the calculated HKUST-1 is provided in Figure S1. Slight differences in crystallinity were also noted, such as the presence of broad peaks in the synthesized HKUST-1. These have been attributed to defects or dislocations occurring within the bulk crystals [33] during crystal growth. Based on the match in PXRD patterns, synthesis of HKUST-1 was assumed to have been successful.

Upon modification to Mo1 via PSM, there is a reduction in crystallinity, shown by the amorphous character of the region from  $2\theta = 10 - 30^\circ$ . Similar changes in diffraction peaks in this region have been observed for other HKUST-1-Mo POM-MOFs [34]. This indicates an expansion in the framework possibly due to molybdenum POMs encapsulated in the voids [34], showing that impregnation was successful and also resulted in partial distortion of the HKUST-1 crystals [35]. Despite partial distortion, Mo1 is still iso-structural to HKUST-1 as shown by the existence of matching peaks, such as those at  $2\theta = 27^\circ$ ,  $29^\circ$ , and  $36^\circ$ .

Mo2 displays a shift to smaller  $2\theta$  values ( $30-24^\circ$ ), confirming incorporation of the POMs. The pattern, however, is characterized by intense sharp peaks at  $22^\circ$ ,  $23^\circ$ ,  $24^\circ$ , and  $33^\circ$  (all absent in HKUST-1), suggesting that a new product results which has its own unique crystal structure, different from HKUST-1.

To aid in confirmation of successful guest inclusion of the Mo POMs, a comparison of the product PXRD with that of the guest is often conducted [36]. For this work,

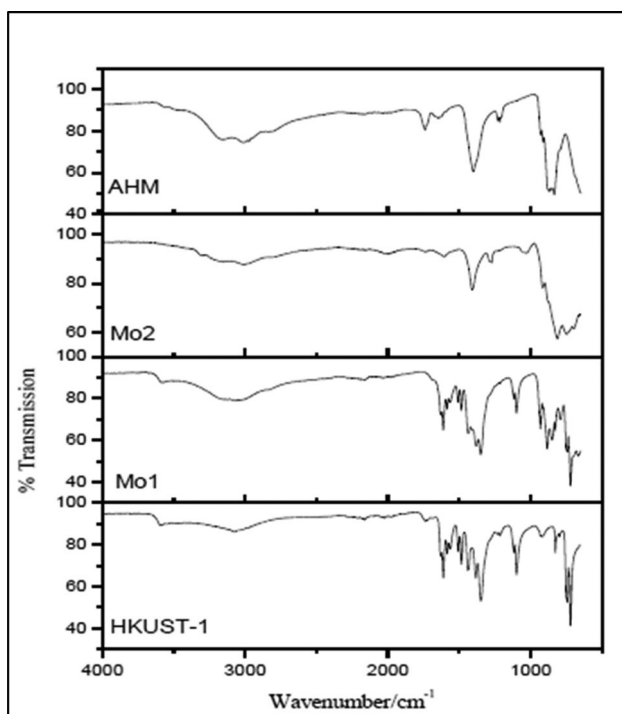


**Figure 2.** FTIR spectra of Mo-HKUST-1 MOFs.

since ammonium heptamolybdate tetrahydrate (AHM) is the guest species, the calculated PXRD for pure AHM was used for comparison [37]. From Figure 1, both Mo2 and Mo1 display characteristic peaks at  $22^\circ$ ,  $23^\circ$ ,  $24^\circ$ ,  $28^\circ$ ,  $31^\circ$ , and  $32^\circ$  which are also observed with pure AHM [38]. This suggests the POM structure is maintained in both Mo1 and Mo2.

### 3.2. Characterization by FTIR

FTIR was used to further investigate the effects of modification on HKUST-1. MOFs of polybenzoic acids tend to display peaks in the carbonyl region. The as-synthesized HKUST-1 displays bands between  $1700$  and  $1400\text{ cm}^{-1}$  (Figure 2), which is in agreement with the published literature on HKUST-1 [13–18]. Its significant bands were at  $1611$ ,  $1585$ ,  $1484$ ,  $1438$ , and  $1400\text{ cm}^{-1}$  for the asymmetric and symmetric regions. It also displays a broad band at  $3072\text{ cm}^{-1}$  which could be due to absorbed water.

When working with pure AHM, the fundamental Mo–O symmetric stretches normally occur between  $1000$  and  $400\text{ cm}^{-1}$  [39–41]. The bands at  $990$ – $957\text{ cm}^{-1}$  are normally ascribed as  $\nu_{\text{as}}\text{Mo}=\text{O}$  stretching vibrations, those around  $880$  and  $818\text{ cm}^{-1}$  are the stretching vibrations of Mo–O–Mo entity and the complex band centered at  $620\text{ cm}^{-1}$  involves the stretch of oxygen linked to three metal ions [39, 42–45]. Similar behavior is observed in the FTIR spectra of both Mo1 and Mo2. Mo1 shows strong bands at  $970$ ,  $913$ , and  $836\text{ cm}^{-1}$  while Mo2 shows bands at  $913$  and  $819\text{ cm}^{-1}$ , confirming the presence of the fundamental Mo POM stretches in both compounds. The

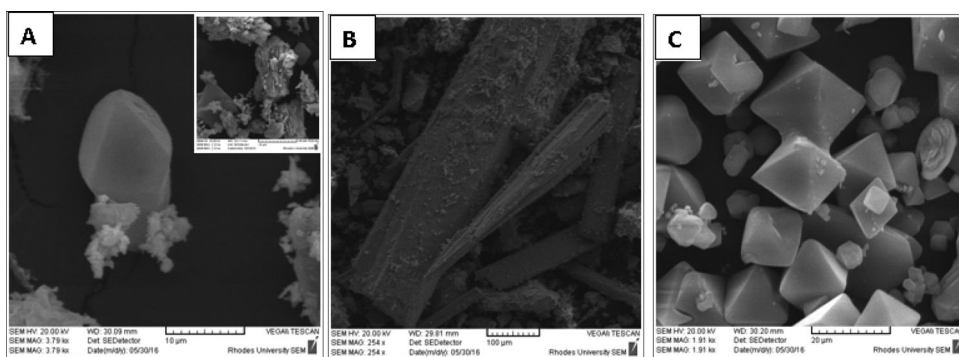


**Figure 3.** SEM images of Mo1 (A), Mo2 (B), and HKUST-1 (C).

slight differences in their values and shifts to lower wavenumbers suggest that the POMs are in different chemical environments and that there may be reduced Mo centers bound to ligands [46].

The spectra for the Mo doped-HKUST-1 POM-MOFs are very similar between 1700 and  $1400\text{ cm}^{-1}$ . Both Mo1 and Mo2 show broad bands ( $3157$ ,  $2996$ , and  $3076\text{ cm}^{-1}$ ) which suggests the presence of water. When working with pure ammonium heptamolybdate POMs, bands for weakly bonded and structurally intercalated ammonium ions were observed between  $3291$  and  $3176\text{ cm}^{-1}$  and their corresponding bonding vibrations in the region  $1458$  to  $1401\text{ cm}^{-1}$  [45]. In Mo1 and Mo2 bands were observed at  $3179\text{ cm}^{-1}$  and  $3205\text{ cm}^{-1}$ , respectively, ascribed to ammonium ions. Mo1 shows shifts to higher wavenumbers for the asymmetric stretch (from  $1611$  to  $1615\text{ cm}^{-1}$ ) and lower wavenumbers for the symmetric stretch ( $1438$  to  $1403\text{ cm}^{-1}$ ), suggesting a change in coordination occurred. Most of the bands in this region have reduced intensity or are masked by the prominent ammonium bending vibrations ( $1585$ ,  $1507$ , and  $1484\text{ cm}^{-1}$ ), suggesting a change in structure. The shift also suggests a reduction in bond strength between copper and BTC due to interactions with the molybdenum POMs. Despite differences in intensity, characteristic bands for HKUST-1 are also seen in Mo1, and this has been taken by previous researchers as an indication that the POMs are encapsulated in the host material [47].

Mo2 displays similar shifts as Mo1 for both the asymmetric and symmetric carbonyl stretches but at lower wavenumbers (from  $1611$  to  $1608\text{ cm}^{-1}$ , from  $1400 - 1383\text{ cm}^{-1}$ ,  $1098 - 1032\text{ cm}^{-1}$ ), suggesting stronger coordination in the solvothermal product. The band at  $1098\text{ cm}^{-1}$  is present in HKUST-1 and Mo1 (as a shoulder) but absent in Mo2, suggesting that the POMs are incorporated differently in the HKUST-1.

### 3.3. SEM

The different morphologies from the electrode modification using different MOFs/POM-MOFs were examined by scanning electron microscopy (Figure 3 and Supplementary Information, Figure S2). Electrode surface morphology is essential as modification is expected to enhance electrocatalytic surface area and hence maximize analyte-catalyst interaction. HKUST-1 shows octahedral crystals which are well defined, have a smooth surface and particle size of  $6\text{--}15\text{ }\mu\text{m}$  (Figure 3(C)) [13, 25, 35, 48].

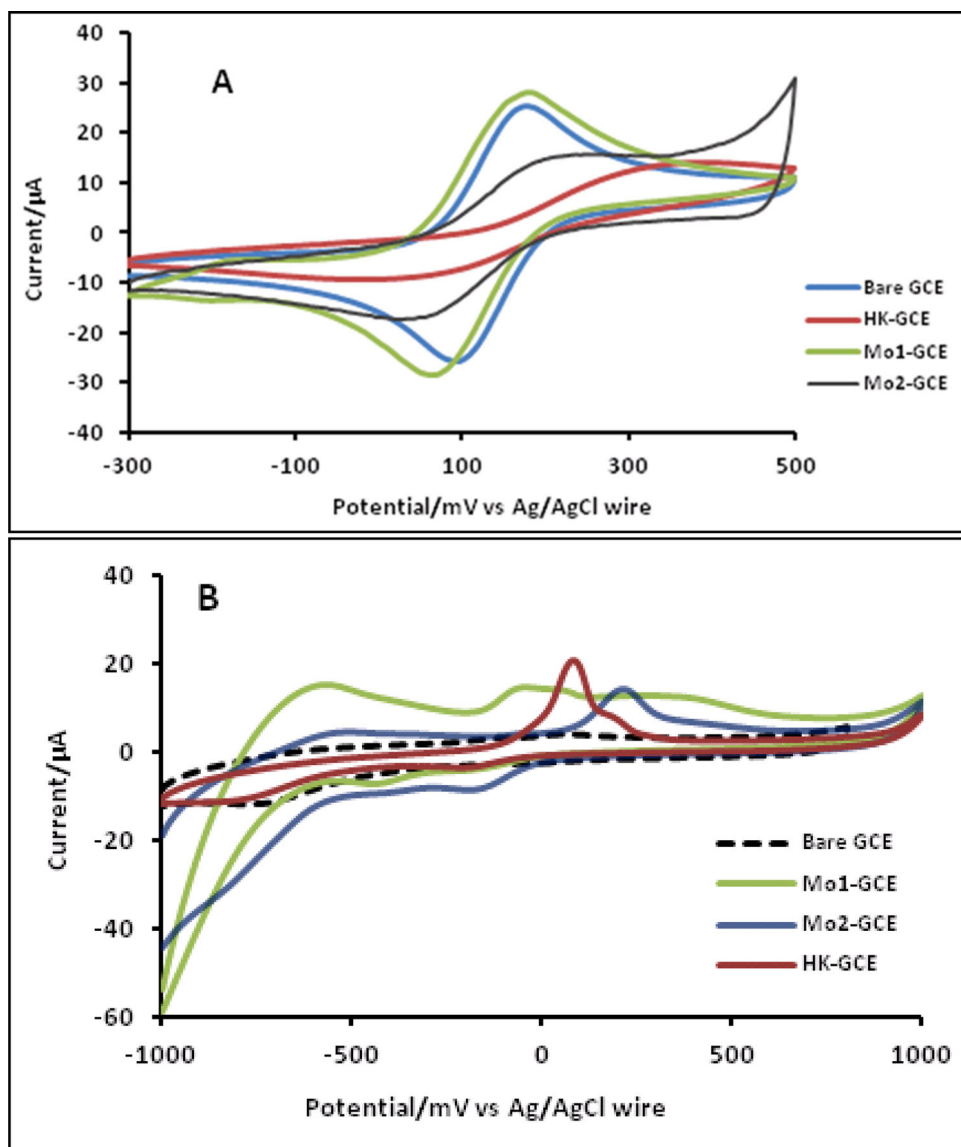


**Figure 4.** Cyclic voltammograms of the bare and modified electrodes in (A) 1 mM  $[\text{Fe}(\text{CN})_6]^{3-/4-}$  and (B) pH 4 buffer at scan rate 100 mV/s.

Smooth surfaces however lead to reduced interactions and thus compromised catalysis. After post-synthetic modification to Mo1, the octahedral shape of HKUST-1 is still maintained but with “cauliflower-like” particles adhered to the surface (insert [Figure 3\(A\)](#)). Similar changes in surface decoration have been observed previously [47] and this behavior was taken to represent successful modification.

Contrary to Mo1, Mo2 shows a total loss of the octahedral shape characteristic of HKUST-1. Its structure consists of rectangular blocks with very fine particles on its surface ([Figure 3\(B\)](#)). The size increases from about 12 to 100 µm for the width of the blocks. This change in shape and size is consistent with phase changes observed in



ammonium heptamolybdate exposed to such temperatures [45, 49]. It is also consistent with the collapse of HKUST-1 observed upon repeated voltammetric cyclisation of HKUST-1 in ethanolic sodium sulfate saturated solution [50]. The SEM micrographs suggest that PSM by impregnation preserved the HKUST-1 octahedral shape while the one-pot approach resulted in formation of a totally different crystal structure. This supports our earlier suggestion that the Mo POMs are incorporated differently; in Mo1 the Mo POMs are encapsulated in the HKUST-1 pore cavity whereas in Mo2 they are incorporated in the framework structure.

### 3.4. Electrochemical characterization of modified electrodes

Electrochemical characterization was performed to gain insight into the interfacial electrochemical behavior between the electrode and the electrolyte in an electrochemical cell [51]. Each MOF was used to modify a glassy carbon electrode and then characterized using cyclic voltammetry to evaluate their electrochemical reactivities. Figure 4(A) shows cyclic voltammograms for the modified and unmodified electrodes in 1 mM  $\text{Fe}(\text{CN})_6^{3-/4-}$  in (a very efficient electron exchange redox media [52, 53]) 0.1 M KCl from  $-0.3$  to  $0.5$  V. The peak potential separation ( $\Delta E$ ) for a reversible system such as  $\text{Fe}(\text{CN})_6^{3-/4-}$  is a good measure of the electron transfer ability of the electrode with lower values depicting a good electron transfer ability [27, 54]. The modified POM-MOF electrodes are in the following order: HK-GCE (0.226 V) > Mo2-GCE (0.132 V) > Mo1-GCE (0.110 V) > Bare GCE (0.078 V) (Table 1).

Thus, electrode modification reduced the electrodes' electron transfer ability compared to that of the Bare GCE electrode. However, comparing the different modifiers revealed that POM-MOF modified electrodes (Mo1-GCE and Mo2-GCE) had a lower  $\Delta E$  compared to the MOF modified electrode (HKUST-1), suggesting that Mo doping improved electron transfer, indicating catalytic superiority of Mo POMs to HKUST-1 as alluded to earlier in this work.

The surface roughness factors for the modified electrodes were determined using  $[\text{Fe}(\text{CN})_6]^{3-/4-}$  redox system and applying Randles–Sevcik [35] Eq. (1) for reversible systems:

$$I_p = 2.69 \times 10^5 n^{3/2} A C D^{1/2} \nu^{1/2} \quad (1)$$

where  $I_p$ ,  $n$ ,  $A$ ,  $C$ ,  $D$ , and  $\nu$  are the peak current, the number of electrons involved, the electrode surface area, the concentration of  $[\text{Fe}(\text{CN})_6]^{3-/4-}$ , the diffusion coefficient of  $[\text{Fe}(\text{CN})_6]^{3-/4-}$ , and the scan rate, respectively.

From the  $D$  value for  $\text{K}_3[\text{Fe}(\text{CN})_6] = 7.6 \times 10^{-6} \text{ cm}^2 \text{ s}^{-1}$  [55] and  $n=1$ , the surface roughness factors (ratio of  $I_{pa}$  experimental/ $I_{pa}$  theoretical; shown in Table 1) were determined for all the probes and the corresponding effective electrode areas {roughness factor  $\times$  theoretical surface area ( $0.071 \text{ cm}^2$ )} were determined and used for the calculation of surface coverage, Eq. (2) [35],

$$\Gamma = \frac{Q}{nFA} \quad (2)$$

where  $\Gamma$  is the film surface coverage,  $Q$  is the charge under the oxidation peak in the supporting electrolyte (Figure 4(B)),  $n$  is the number of transferred electrons,  $F$  is the

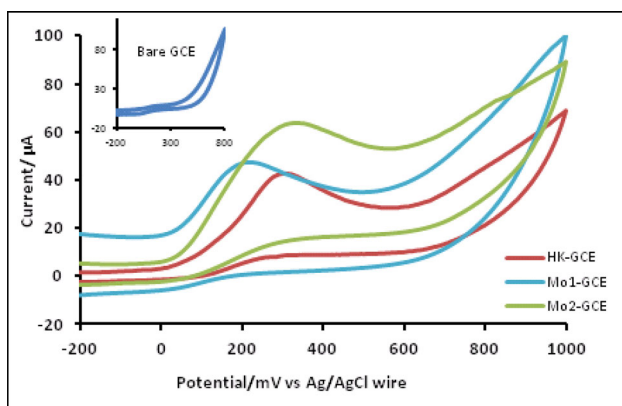


**Figure 5.** Cyclic voltammograms of the modified electrodes (and bare GCE (insert)) in 10 mM L-cysteine at 100 mV/s scan rate; pH 4 buffer.

Faraday constant, and  $A$  is the effective area of the electrode. The surface coverage follows the order Mo1-GCE > Mo2-GCE > HK-GCE. Figure 4(B) shows the CVs for the bare and modified electrodes in pH 4 buffer solutions. The bare GCE displays no peak. Upon modification, HK-GCE and Mo2-GCE both display well resolved peaks at 195 to 60 mV with the highest signal at 20  $\mu$ A, belonging to HK-GCE. Mo1-GCE has a less defined peak in buffer.

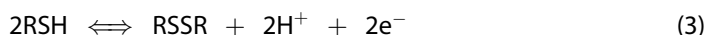
### 3.5. L-Cysteine detection

#### 3.5.1. Cyclic voltammetry

During an electrocatalytic reaction, electron exchange is followed by a current signal at the potential equivalent to the activation energy. As such the appearance of a current peak is evidence of the occurrence of a reaction involving an analyte. Cyclic voltammetry has been used in various studies of this nature. In this work all modified electrodes and the bare GCE were investigated by cyclic voltammetry in the potential window  $-200$  to  $1000$  mV. The bare GCE did not display a peak while all the modified electrodes exhibited electrocatalytic oxidation of L-cysteine with good signal strengths (Figure 5 and Table 1). The observed oxidation peak potential window was  $0.205 - 0.328$  V, which is characteristic for L-cysteine oxidation [4]. L-cysteine has also been detected on a gold film modified carbon electrode at similar pHs (4.86), but at much higher potentials, attesting to the superiority of the present probes and their potential in the detection of the biomolecule in acidic media [23].

In terms of oxidation potential, the electrodes followed the order Mo2-GCE ( $0.328$  V) > HK-GCE ( $0.283$  V) > Mo1-GCE ( $0.205$  V). Since the bare GCE did not exhibit a peak, it can be concluded that modification with HKUST-1, Mo1, and Mo2 resulted in electrodes with an ability to detect L-cysteine. Mo1-GCE was able to do this at the lowest potential while Mo2-GCE gave the highest signal (almost twice that of HK-GCE), Table 1. This behavior can be attributed to the higher surface roughness values and subsequent effective surface area determined electrochemically for the modified electrodes.

L-cysteine can be oxidized to cystine via Eq. (3) [23, 40],



where RSH=L-cysteine and RSSR = cystine.

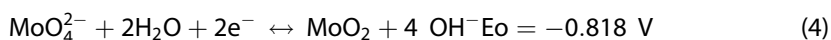
Electrocatalytic oxidation can be either due to interaction with the cavity or the framework [56]. HKUST-1 has coordinatively unsaturated  $\text{Cu}^{2+}$  sites [18] that are available for oxidation of L-cysteine. It is proposed that during L-cysteine oxidation, the mechanism involves reduction of  $\text{Cu}^{2+}$  to  $\text{Cu}^0$ . This normally occurs at  $E^0 = 0.34\text{ V}$ , however according to Giri and Sarkar [57], this value can also be as low as  $E^0 = 0.25\text{ V}$  in very alkaline solutions, suggesting that pH affects electrode potentials [58]. In this work, we propose that reduction of  $\text{Cu}^{2+}$  to  $\text{Cu}^0$  occurred at  $E^0 = 0.283\text{ V}$ .

When Mo is incorporated, there is an increase in available metal centers (due to the  $\text{Mo}_6\text{-POM}$ ). At this stage, it is proposed that the Mo is reduced from  $\text{Mo}^{6+}$  to  $\text{Mo}^{4+}$  instead of  $\text{Mo}^{5+}$  (due to the absence of the dark blue color associated with Mo-blues). POMs have been reported to easily and rapidly undergo one or two electron reductions reversibly in electrocatalysis [20].

It is important to note that the modification method used has a direct bearing on the efficiency of the catalyst as can be seen from the different oxidation potentials. The following is proposed:

1. A one-pot solvothermal approach reduces the number of available active sites, possibly because there is saturation of the metal coordination sites ( $\text{Mo}^{6+}$  and  $\text{Cu}^{2+}$ ) in formation of the framework. This results in electron transfer occurring at higher potentials (compare HK-GCE (0.283 V) to (Mo2-GCE (0.328 V)).
2. PSM at room temperature results in an increase in catalytic sites (compare HK-GCE (0.283 V) to (Mo1-GCE (0.205 V)).

The electrode behavior suggests that PSM allows for both cavity (encapsulated POM) and framework (Cu) mechanisms to be employed [59], hence resulting in the observed lower potential for Mo1-GCE. Electro-reduction of L-cysteine is usually difficult, suggesting that the reaction is irreversible. Reversibility can be either chemical or electrochemical in nature. Chemical irreversibility occurs when products rapidly transform or decompose into another form and prohibit return to original materials [60, 61]. Electrochemical irreversibility is often due to the kinetics of electron transfer being slow [54]. We propose that irreversibility could have been due to either chemical or electrochemical means. L-cysteine has been known to rapidly transform to the oxidized species by undergoing an irreversible chemical reaction, a phenomenon suggested previously [62]. It could also be due to the high energy requirements for oxidation of  $\text{MoO}_2$  (Eq. (4)) back to  $\text{Mo}^{6+}$ , making the reaction almost irreversible [9]. In such instances, an overpotential has to be applied to overcome the activation barrier of the slow electron transfer reaction [63].



Electrode stability was investigated by running 20 successive cyclic voltammograms in 10 mM L-cysteine (Figures 6(A–C)). The Mo2-GCE and HK-GCE are fairly stable and continue to detect L-cysteine, with good signal strength after 20 cycles. Mo1-GCE is not as stable and loses its ability to detect with consistency after about 10 cycles. The

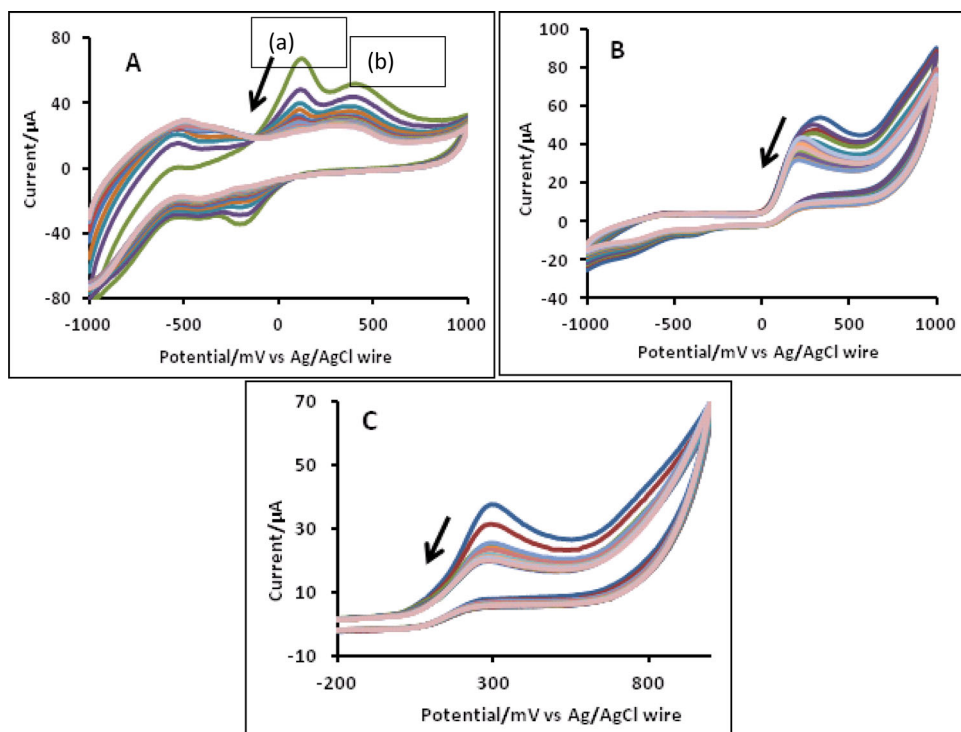


**Figure 6.** Cyclic voltammograms (20 successive scans) of Mo1-GCE (A), Mo2-GCE (B), and HK-GCE (C) in 10 mM L-cysteine. Scan rate of 100 mV/s. pH 4 buffer.

reaction for Mo1-GCE appears to shift, from irreversible to reversible. This could be due to loss of the catalyst (Mo POM) encapsulated in the MOF with cycling [64]. We tentatively suggest that the peaks (a) and (b) are for Mo1 and L-cysteine, respectively.

### 3.5.2. Kinetic studies

The effect of scan rates on the modified electrodes was investigated in L-cysteine. The change in the scan rate is accompanied by a shift in peak potential which is suggestive of an irreversible reaction during oxidation of L-cysteine on the modified electrode surface (Figure 7(A)). The relationship between oxidation peak potential and log of scan rate (Figure 7(B)) for an irreversible diffusion-controlled process is given by Eq. (5) [27],

$$E_p = \frac{2.303RT}{2(1-\alpha)n_\alpha F} \log v + K \quad (5)$$

where  $\alpha$  is the electron transfer coefficient,  $n_\alpha$  is the number of electrons involved in the rate determining step,  $v$  is the scan rate,  $K$  is a constant,  $R$  is the universal gas constant, and  $T$  is the temperature (298 K).

A plot for peak current increases linearly with the square root of scan rate ( $v^{1/2}$ ), an indication of electrochemical processes that are diffusion controlled [27]. This behavior is observed for Mo2-GCE (Figure S4, Supplementary Information). The plots for HK-GCE (Figure 7(C)) and Mo1-GCE (Figure S3, Supplementary Information), however, show slight deviations from linearity, suggesting either electrochemical quasi-reversibility or that electron transfer is occurring via surface adsorbed species [65].

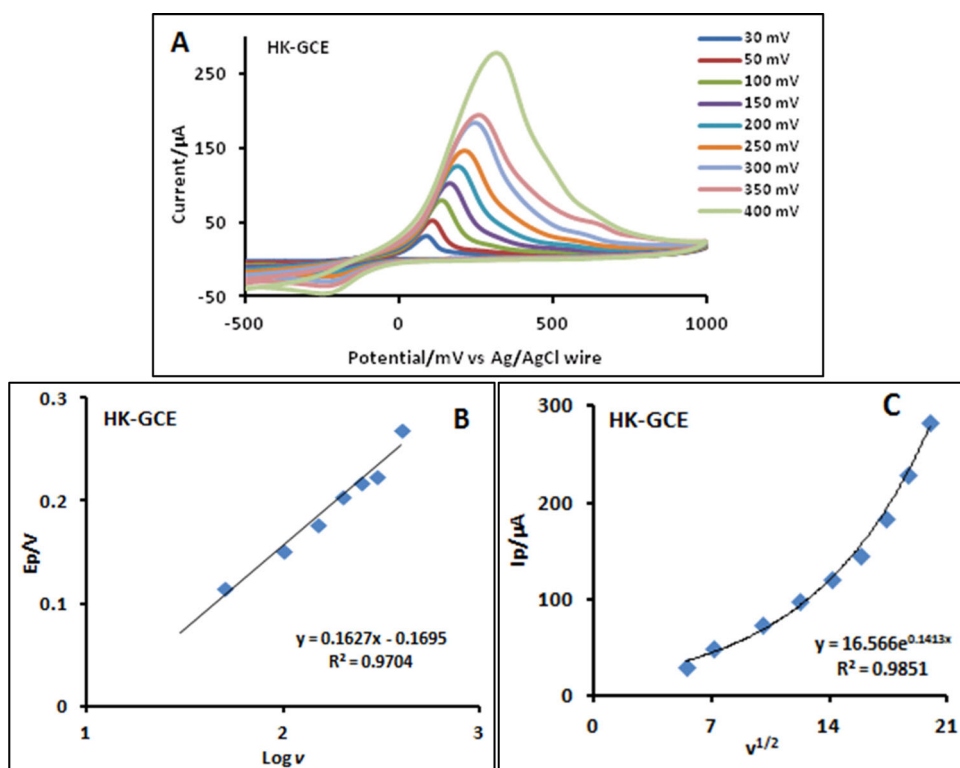


**Figure 7.** Cyclic voltammograms for detection of L-cysteine at different scan rates (A), the corresponding plots of oxidation  $E_p$  vs.  $\text{Log } \nu$  (B) and of oxidation  $I_p$  vs.  $\nu^{1/2}$  (C) in 10 mM L-cysteine of HK-GCE; pH 4 buffer.

For an electrochemical quasi-reversible process, a shift is observed in peak-to-peak separation with scan rate, whereas for surface adsorbed species, there is no observable shift. Analysis of the plots of current versus scan rate all show shifts; this suggests the deviations from linearity observed for HK-GCE and Mo1-GCE are a result of the process being electrochemically quasi-reversible. All plots also show an increase in  $\Delta E$  with increase in scan rate because faster scan rates lead to a decrease in the size of the diffusion layer; as a consequence, higher currents are observed [65].

Plots of  $E_p$  versus  $\text{log } \nu$  (Figure 7(B)) were used to determine the Tafel slopes. The Tafel slopes for HK-GCE, Mo1-GCE, and Mo2-GCE all gave high values (326 mV/decade, 183 mV/decade, and 213 mV/decade, respectively). This indicates adsorption complications which can be caused by the presence of either the products or intermediates on the modified electrode surface [39]. Such high Tafel slopes (greater than normal; 30 – 120 mV/decade) have also been linked to chemical reactions coupled to electrochemical steps or electrode passivation. High Tafel slopes are also an indication that Volher's discharge reaction is rate limiting [66]. Materials with very high surface area to volume ratios, like activated carbon [67], metal nanoparticles [68], and MOFs [69, 70] give high Tafel slopes; hence it is not surprising that the current study deals with POM-MOFs.

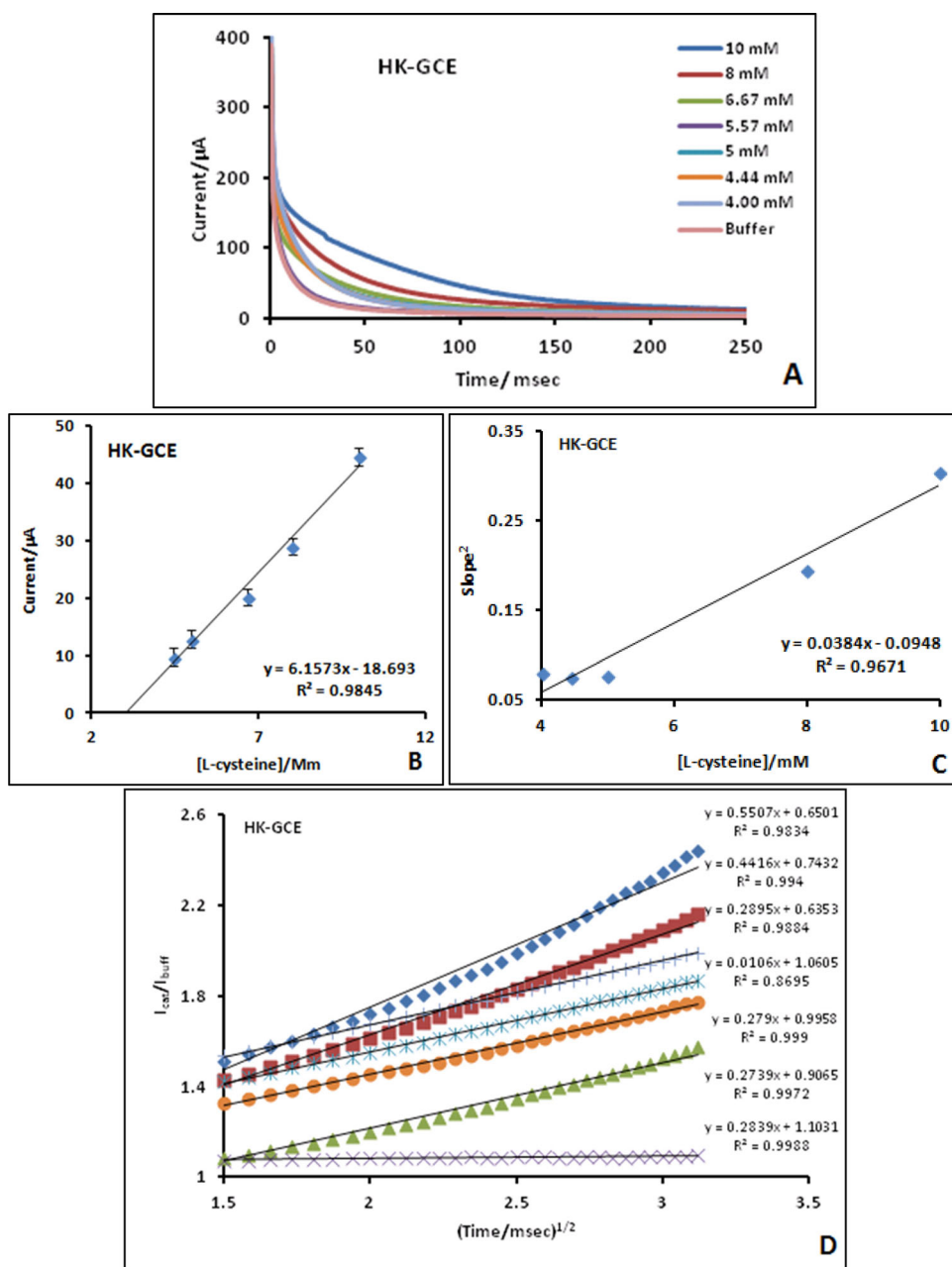


**Figure 8.** Chronoamperograms, plots of  $I_{\text{cat}}/I_{\text{buf}}$  vs.  $t^{1/2}$  (10, 8.0, 6.67, 5.71, 5.0, 4.44, 4.0, and at 3.64 mM), calibration curves and plots of  $\text{slope}^2$  vs. [L-cysteine] determined using chronoamperometry for HK-GCE.

### 3.6. Chronoamperometry

Chronoamperometry was used to determine nanoprobe sensitivity, rate constants and detection limits. Within the first 0.1 s (on average), the catalytic current is dominated

**Table 2.** Comparative LODs for electrochemical oxidation of L-cysteine using different catalytic systems.

Electrode	pH	LOD	Range	Sensitivity	K	Reference
Mo1-GCE	4	$3.07 \times 10^{-7}$ M	3–10 mM	4.5 $\mu$ A/mM	$2.2 \times 10^4$ M <sup>-1</sup> s <sup>-1</sup>	This work
Mo2-GCE	4	$3.47 \times 10^{-7}$ M	3–10 mM	25 $\mu$ A/mM	$2.2 \times 10^4$ M <sup>-1</sup> s <sup>-1</sup>	This work
HK-GCE	4	$3.03 \times 10^{-7}$ M	3–10 mM	6.1 $\mu$ A/mM	$2.2 \times 10^4$ M <sup>-1</sup> s <sup>-1</sup>	This work
Bo-CNT-GCE <sub>x</sub>	7.4	$2.60 \times 10^{-7}$ M	0.07–2 mM	25.3 nA/mM	–	[62]
Pt-CNT	7.4	$3.00 \times 10^{-7}$ M	0.05–0.1 mM	–	–	[71]
FeDCM-CPE	8	$2.60 \times 10^{-5}$ M	0.3–2.2 mM	–	$8.3 \times 10^3$ cm <sup>3</sup> mol <sup>-1</sup> s <sup>-1</sup>	[72]
Cu-CoHCF-CPE	2	$5.00 \times 10^{-6}$ M	0.06–1 mM	–	$4.6 \times 10^6$ cm <sup>3</sup> mol <sup>-1</sup> s <sup>-1</sup>	[73]
CoTAPc-MWCNT-GCE	4	$2.80 \times 10^{-7}$ M	0.04–0.4 mM	7.0 mA/mM	$2.2 \times 10^5$ M <sup>-1</sup> s <sup>-1</sup>	[74]

by electrooxidation of L-cysteine (Figure 8(A) and Supplementary Information, Figures S5 and S6) before it reaches steady-state. The sensitivity (in  $\mu$ A/mM) of the probes followed the order Mo1-GCE (4.4919) < HK-GCE (6.1439) < Mo2-GCE (25.329) (Figure 8(B) and Supplementary Information, Figures S5 and S6).

According to the literature, the rate constant can be evaluated using Eq. (6),

$$\frac{I_{\text{cat}}}{I_{\text{buf}}} = \frac{\gamma^{1/2}(\pi^{1/2}\text{erf}(\gamma^{1/2}) + \exp(-\gamma))}{\gamma^{1/2}} \quad (6)$$

where  $I_{\text{cat}}$  and  $I_{\text{buf}}$  are the currents on the modified GCE in the presence and absence of L-cysteine, respectively,  $\gamma = kC_0t$  ( $C_0$  is the bulk concentration of L-cysteine) and erf is the error function.

In cases where  $\gamma > 2$ , the error function is almost equal to 1 and Eq. (6) can be reduced to Eq. (7),

$$\frac{I_{\text{cat}}}{I_{\text{buf}}} = \gamma^{1/2}\pi^{1/2} = \pi^{1/2}(kC_0t)^{1/2} \quad (7)$$

where  $k$  is the catalytic rate constant,  $C_0$  is the bulk concentration of L-cysteine, and  $t$  is time elapsed in seconds.

Figure 8(D) (and Supplementary Information, Figures S5 and S6) shows the plots of  $I_{\text{cat}}/I_{\text{buf}}$  versus  $t^{1/2}$  (Eq. (7)) for L-cysteine oxidation. The plots were used to calculate the rate constants and these are represented by Eqs. 8(a–c) for HK-GCE, Mo1-GCE, and Mo2-GCE, respectively. The slope is equal to  $\pi k$  where  $k$  is the rate constant.

$$y = 0.0384[\text{l-cysteine}] \left( \frac{\text{s}^{-1}}{\text{mM}} \right) - 0.0948 \text{ s}^{-1} \quad R2 = 0.9671; \quad (8a)$$

$$y = 0.0697[\text{l-cysteine}] \left( \frac{\text{s}^{-1}}{\text{mM}} \right) - 0.0563 \text{ s}^{-1}; \quad R2 = 0.943 \quad (8b)$$

$$y = 0.0182[\text{l-cysteine}] \left( \frac{\text{s}^{-1}}{\text{mM}} \right) - 0.0539 \text{ s}^{-1}; \quad R2 = 0.9694 \quad (8c)$$

The rate constants were  $1.22 \times 10^4$  M<sup>-1</sup> s<sup>-1</sup>,  $2.2 \times 10^4$  M<sup>-1</sup> s<sup>-1</sup>, and  $5.8 \times 10^3$  M<sup>-1</sup> s<sup>-1</sup> for HK-GCE, Mo1-GCE, and Mo2-GCE, respectively. This compares well with those obtained on other modified electrodes [27, 40, 62]. The electrocatalytic oxidation peak current of L-cysteine showed linear dependence on the L-cysteine concentration obtained in the range 3 mM –  $1.0 \times 10^{-2}$  M.

Following triplicate chronoamperometric measurements, limits of detection (LOD) values were calculated using the  $3\sigma$  notation, and using the calibration curves (Figure

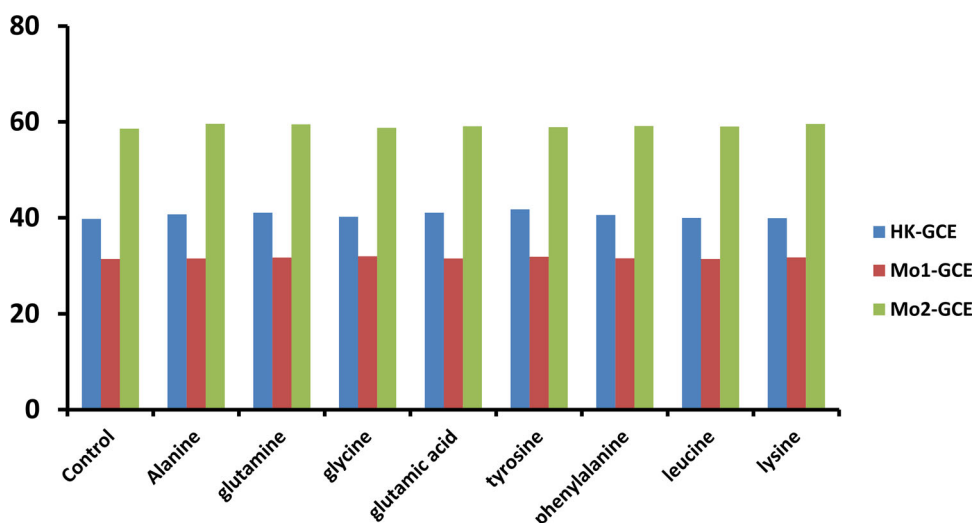


**Figure 9.** Effects of essential and nonessential amino acids on detection of L-cysteine on the modified electrode surface. Control comprises 10 mM L-cysteine while the other test solutions have threefold concentration of individual amino acids in addition to the aforementioned L-cysteine concentration.

**Table 3.** Percentage background corrected current (%) change of coexisting essential and nonessential amino acids on the detection of L-cysteine on modified electrodes.

	HK-GCE	Mo1-GCE	Mo2-GCE
Alinine	2.4	0.3	1.7
Glutamine	3.3	1.0	1.5
Glycine	1.1	1.8	0.3
Glutamic acid	3.3	0.3	0.9
Tyrosine	3.3	1.4	0.5
Phenylalanine	2.1	0.4	0.9
Leucine	0.6	0.0	0.9
Lysine	0.4	1.0	1.7

8(B)). LODs followed the order HK-GCE < Mo1-GCE < Mo2-GCE. All values are within the range often found in biological fluids (0.5–680  $\mu$ M, Table 2) such as urine and plasma [75]. Compared to HK-GCE though, both Mo1-GCE and Mo2-GCE LODs were slightly higher, suggesting that molybdenum decreased the sensitivity of the electrodes for L-cysteine detection.

### 3.7. Sensor selectivity

The selectivity of HK-GCE, Mo1-GCE, and Mo2-GCE towards the detection of L-cysteine was against a number of essential and nonessential physiological amino acids (Figure 9). A threefold interferent concentration was used as a test solution and the background corrected currents are shown in Figure 9. The obtained signal in the absence of interferent is given as the control. The signal obtained after the interferents were individually added were used to determine the percentage background corrected current change as captured in Table 3. The results show a slight signal enhancement in the presence of threefold interferent concentrations. This is plausible since L-cysteine



is better detected through the thio functionality absent in other amino acids [76]. The changes in intensity are, however, very low and hence there is negligible interference.

## 4. Conclusion

Glassy carbon electrodes modified with HKUST-1, Mo1, and Mo2 were employed for detection of L-cysteine. Mo1-GCE gave the best catalytic activity with a rate constant of  $2.2 \times 10^4 \text{ M}^{-1} \text{ s}^{-1}$  and relatively low detection limits of  $3.07 \times 10^{-7} \text{ M}$ . The low detection limits and wide range of linearity points to these probes as a promising platform for L-cysteine sensing. The probes also showed high selectivity toward L-cysteine detection in the presence of other amino acids, hence very suitable candidates for L-cysteine detection in physiological samples.

## Disclosure Statement

No potential conflict of interest was reported by the authors.

## Funding

This work was supported by the Department of Science and Technology (DST) and National Research Foundation (NRF), South Africa through DST/NRF South African Research Chairs Initiative for Professor of Medicinal Chemistry and Nanotechnology (UID 62620) as well as Rhodes University South Africa.

## ORCID

Munyaradzi Shumba  <http://orcid.org/0000-0002-7462-708X>

Tebello Nyokong  <http://orcid.org/0000-0002-4590-9926>

## References

- [1] X. Hu, Y. Lu, F. Dai, C. Liu, Y. Liu. *Microporous Mesoporous Mater.*, 170, 36 (2013).
- [2] H. Al-Kandari, S. Al-Kandari, A.M. Mohamed, F. Al-Kharafi, A. Katrib. *Mod. Res. Catal.*, 4, 36 (2015).
- [3] H. Lü, Y. Zhang, Z. Jiang, C. Li. *Green Chem.*, 12, 1954 (2010).
- [4] A. Nisar, Y. Lu, J. Zhuang, X. Wang. *Angew. Chem. Int. Ed. Engl.*, 50, 3187 (2011).
- [5] A. Sakakura, R. Kondo, K. Ishihara. *Org. Lett.*, 7, 1971 (2005).
- [6] B. Liu, J. Yang, G.-C. Yang, J.-F. Ma. *Inorg. Chem.*, 52, 84 (2013).
- [7] B. Keita, E. Abdeljalil, L. Nadjo, R. Contant, R. Belghiche. *Langmuir*, 22, 10416 (2006).
- [8] B. Nohra, H. El Moll, L.M. Rodriguez Albelo, P. Mialane, J. Marrot, C. Mellot-Draznieks, M. O'Keeffe, R. Ngo Biboum, J. Lemaire, B. Keita, L. Nadjo, A. Dolbecq. *J. Am. Chem. Soc.*, 133, 13363 (2011).
- [9] C.-Y. Sun, S.-X. Liu, D.-D. Liang, K.-Z. Shao, Y.-H. Ren, Z.-M. Su. *J. Am. Chem. Soc.*, 131, 1883 (2009).
- [10] G. Mehlanan, S.A. Bourne, G. Ramon. *CrystEngComm*, 16, 8160 (2014).
- [11] G. Mehlanan, S.A. Bourne, G. Ramon. *Dalton Trans.*, 41, 4224 (2012).
- [12] E. Barea, C. Montoro, J.A.R. Navarro. *Chem. Soc. Rev.*, 43, 5419 (2014).

- [13] K.-S. Lin, A.K. Adhikari, C.-N. Ku, C.-L. Chiang, H. Kuo. *Int. J. Hydrogen Energy*, 37, 13865 (2012).
- [14] H. Yang, S. Orefuwa, A. Goudy. *Microporous Mesoporous Mater.*, 143, 37 (2011).
- [15] J.L. Zhuang, D. Ceglarek, S. Pethuraj, A. Terfort. *Adv. Funct. Mater.*, 21, 1442 (2011).
- [16] J.M. Zamaro, N.C. Perez, E.E. Miro, C. Casado, B. Seoane, C. Tellez, J. Coronas. *Chem. Eng. J.*, 195–196, 180 (2012).
- [17] Y. Chen, X. Huang, X. Feng, J. Li, Y. Huang, J. Zhao, Y. Guo, X. Dong, R. Han, P. Qi, Y. Han, H. Li, C. Hu, B. Wang. *Chem. Commun. (Camb.)*, 50, 8374 (2014).
- [18] S. Bordiga, L. Regli, F. Bonino, E. Groppo, C. Lamberti, B. Xiao, P.S. Wheatley, R.E. Morris, A. Zecchina. *Phys. Chem. Chem. Phys.*, 9, 2676 (2007).
- [19] Y. Wang, H. Ge, G. Ye, H. Chen, X. Hu. *J. Mater. Chem. B*, 3, 3747 (2015).
- [20] S.-S. Wang, G.-Y. Yang. *Chem. Rev.*, 115, 4893 (2015).
- [21] H. Hosseini, H. Ahmar, A. Dehghani, A. Bagheri, A. Tadjarodi, A. Reza. *Biosens. Bioelectron.*, 42, 426 (2013).
- [22] N.C. Plaza, M.R. Gracia-Galbis, R.M. Martinez-Espinosa. *Molecules*, 23, 1 (2018).
- [23] L.-H. Wang, W.-S. Huang. *Sensors (Basel)*, 12, 3562 (2012).
- [24] J. Yin, W. Ren, G. Yang, J. Duan, X. Huang, R. Fang, C. Li, T. Li, Y. Yin, Y. Hou, S.W. Kim, G. Wu. *Mol. Nutr. Food Res.*, 60, 134 (2016).
- [25] C. Wei, X. Li, F. Xu, H. Tan, Z. Li, L. Sun, Y. Song. *Anal. Methods*, 6, 1550 (2014).
- [26] M.P. Motaung, P.A. Ajibade. *Int. J. Electrochem. Sci.*, 10, 8087 (2015).
- [27] M. Shumba, T. Nyokong. *Electrochim. Acta*, 196, 457 (2016).
- [28] W. Liu, X.-B. Yin. *Trends Anal. Chem.*, 75, 86 (2016).
- [29] S.S.-Y. Chui, S.M.-F. Lo, J.P.H. Charmant, A.G. Orpen, I.D. Williams. *Science*, 283, 1148 (1999).
- [30] T. Granato, F. Testa, R. Olivo. *Microporous Mesoporous Mater.*, 153, 236 (2012).
- [31] M. Schlesinger, S. Schulze, M. Hietschold, M. Mehring. *Microporous Mesoporous Mater.*, 132, 121 (2010).
- [32] Y. Li, R.T. Yang. *AIChE J.*, 54, 269 (2008).
- [33] P.M. Shafi, A.C. Bose. *AIP Adv.*, 5, 057137 (2015).
- [34] H.-B. Wu, B.-Y. Xia, L. Yu, X.-Y. Yu, X.-W. (David) Lou. *Nat. Commun.*, 6, 6512 (2015).
- [35] S. Abednatanzi, M. Masteri-Farahani, A. Abbasi. *New J. Chem.*, 39, 5322 (2015).
- [36] K.G. Desai, C. Liu, H.J. Park. *J. Microencapsul.*, 23, 79 (2006).
- [37] H.T. Evans, B.M. Gatehouse, P. Leverett. *J. Chem. Soc., Dalton Trans.*, 6, 505 (1975).
- [38] Y.-G. Li, N. Hao, E.-B. Wang, Y. Lu, C.-W. Hu, L. Xu. *Eur. J. Inorg. Chem.*, 2003, 2567 (2003).
- [39] L. Seguin, M. Figlarz, R. Cavagnat, J.C. Lassegues. *Spectrochim. Acta, Part A*, 51, 1323 (1995).
- [40] G. Tsilomelekis, S. Boghosian. *J. Phys. Chem. C*, 115, 2146 (2011).
- [41] K.G. Ravikumar, S. Rajaraman, S. Mohan. *Proc. Ind. Natl. Sci. Acad. U. S. A.*, 51, 368 (1984).
- [42] Y.-G. Li, L.-M. Dai, Y.-H. Wang, X.-L. Wang, E.-B. Wang, Z.-M. Su, L. Xu. *Chem. Commun.*, 2593, (2007).
- [43] S. Tangestaninejad, M. Moghadam, V. Mirkhani, I. Mohammadpoor-Baltork, K. Ghani. *J. Iran. Chem. Soc.*, 5, s71 (2008).
- [44] R. Thouvenot, M. Fournier, R. Franck, C. Rocchiccioli-Deltcheff. *Inorg. Chem.*, 23, 598 (1984).
- [45] A. Chithambararaj, D. Bhagya Mathi, N. Rajeswari Yogamalar, A. Chandra Bose. *Mater. Res. Express*, 2, 055004 (2015).
- [46] G. Nagaraju, C.N. Tharamani, G.T. Chandrappa, J. Livage. *Nanoscale Res. Lett.*, 2, 461 (2007).
- [47] J. Juan-Alcaniz, M.G. Goesten, E.V. Ramos-Fernandez, J. Gascon, F. Kapteijn. *New J. Chem.*, 36, 977 (2012).
- [48] J. Kim, S.-H. Kim, S.-T. Yang, W.-S. Ahn. *Microporous Mesoporous Mater.*, 161, 48 (2012).
- [49] X.-W. Lou, H.-C. Zeng. *Chem. Mater.*, 14, 4781 (2002).
- [50] S.D. Worrall, M.A. Bissett, W. Hirunpinyopas, M.P. Atfield, R.A.W. Dryfe. *J. Mater. Chem. C*, 4, 8687 (2016).

- [51] Y.S. Choudhary, L. Jothi, G. Nageswaran. *Spectroscopic Methods for Nanomaterials Characterization, Electrochemical Characterization, Chapter 2*, Elsevier Inc., Amsterdam, Netherlands, pp. 19–54 (2017).
- [52] V. Svoboda, M. Cooney, BYann Liaw, S. Minteer, E. Piles, D. Lehnert, S. Calabrese Barton, R. Rincon, P. Atanassov. *Electroanalysis*, 20, 1099 (2008).
- [53] A. Morrin, A.J. Killard, M.R. Smyth. *Anal. Lett.*, 36, 2021 (2003).
- [54] A.J. Bard, L.R. Faulkner. *Electrochemical Methods; Fundamentals and Applications*, 2nd edn, John Wiley & Sons, Inc., New York (2001).
- [55] J.J. Gooding, V.G. Praig, E.A.H. Hall. *Anal. Chem.*, 70, 2396 (1998).
- [56] B. Yuan, J. Zhang, R. Zhang, H. Shi, X. Guo, Y. Guo, X. Guo, S. Cai, D. Zhang. *Int. J. Electrochem. Sci.*, 10, 4899 (2015).
- [57] S.D. Giri, A. Sarkar. *J. Electrochem. Soc.*, 163, H252 (2016).
- [58] S.M.A. el Haleem, B.G. Ateya. *J. Electroanal. Chem. Interfacial Electrochem.*, 117, 309 (1981).
- [59] D. Yang, B.C. Gates. *ACS Catal.*, 9, 1779 (2019).
- [60] F.A. Armstrong, J. Hirst. *Proc. Natl. Acad. Sci. U. S. A.*, 108, 14049 (2011).
- [61] M.V. Mirkin, S. Amemiya. *Nanoelectrochemistry*, 4 (2015). doi:[10.1201/b18066](https://doi.org/10.1201/b18066).
- [62] C. Deng, J. Chen, X. Chen, M. Wang, Z. Nie, S. Yao. *Electrochim. Acta*, 54, 32998 (2009).
- [63] F. Scholz. *Electroanalytical Methods: Guide to Experiments and Applications* (2010). doi:[10.1007/978-3-642-02915-8](https://doi.org/10.1007/978-3-642-02915-8).
- [64] A. Pozio, M. De Francesco, A. Cemmi, F. Cardellini, L. Giorgi. *J. Power Sources*, 105, 13 (2002).
- [65] N. Elgrishi, K.J. Rountree, B.D. McCarthy, E.S. Rountree, T.T. Eisenhart, J.L. Dempsey. *J. Chem. Educ.*, 95, 197 (2018).
- [66] C.A. Downes, S.C. Marinescu. *ChemSusChem*, 10, 4374 (2017).
- [67] Z. Hu, M.P. Srinivasan. *Microporous Mesoporous Mater.*, 43, 267 (2001).
- [68] J.N. Sharma, D.K. Pattadar, B.P. Mainali, F.P. Zamborini. *Anal. Chem.*, 90, 9308 (2018).
- [69] J. Duan, S. Chen, C. Zhao. *Nat. Commun.*, 8, 15341 (2017). doi:[10.1038/ncomms15341](https://doi.org/10.1038/ncomms15341).
- [70] N. Kornienko, Y. Zhao, C.S. Kley, C. Zhu, D. Kim, S. Lin, C.J. Chang, O.M. Yaghi, P. Yang. *J. Am. Chem. Soc.*, 137, 14129 (2015).
- [71] S. Fei, J. Chen, S. Yao, G. Deng, D. He, Y. Kuang. *Anal. Biochem.*, 339, 29 (2005).
- [72] J.B. Raoof, R. Ojani, H. Beitollahi. *Electroanalysis*, 19, 1822 (2007).
- [73] A. Abbaspour, A. Ghaffarnejad. *Electrochim. Acta*, 53, 6643 (2008).
- [74] S. Nyoni, T. Mugadza, T. Nyokong. *Electrochim. Acta*, 128, 32 (2014).
- [75] C. Xiao, J. Chen, B. Liu, X. Chu, L. Wu, S. Yao. *Phys. Chem. Chem. Phys.*, 13, 1568 (2011).
- [76] A.H.B. Dourado, F.C. Pastrian, S.I. Cordoba, D.E. Torresi. *An. Acad. Bras. Cienc.*, 90, 607 (2018).